

Received 28 September 2023, accepted 5 December 2023, date of publication 14 December 2023, date of current version 16 January 2024.

Digital Object Identifier 10.1109/ACCESS.2023.3343101

RESEARCH ARTICLE

Improved Velocity Determination Method by the Integration of Multi-GNSS Satellites' Doppler and Phase Observations

YUNLONG ZHANG 

China Railway Design Corporation, Tianjin 300308, China

Tianjin Key Laboratory of Rail Transit Navigation Positioning and Spatio-Temporal Big Data Technology, Tianjin 300308, China

e-mail: 13115311@bjtu.edu.cn

This work was supported in part by the Science and Technology Research and Development Project of China State Railway Group Company Ltd. under Grant P2022X001, and in part by the Tianjin Key Laboratory of Rail Transit Navigation Positioning and Spatio-Temporal Big Data Technology under Grant TKL2023B07.


ABSTRACT Velocity determination as one of the widely used spatial information is essential for the location-based services. Concerned researches about Global Navigation Satellite System (GNSS) velocity determination mainly focus on carrier phase observations, which ignored the merits of multi-type observations transmitted by multi-GNSS satellites. To increase the performances of GNSS velocity determination, the Helmert variance components estimation (VCE) algorithm is introduced into the integration of Doppler and carrier phase observations, moreover a velocity vector constraint is designed with the aid of original phase observations, constructing the condition equation, and inserting into GNSS velocity determination model. According to kinematics experiments, results show that the integrated Doppler and carrier phase observations can obtain cm/s level accuracy for E, N and U directions, with improvements of 94.1%, 93.9% and 89.5% respectively, compared with Doppler-only scheme. However, the obvious accuracy reductions are occurred during the satellite signal obstruction, where the corresponding improvements with 89.7%, 90.1% and 69.4% for E, N and U directions can be obtained. Meanwhile, the constraint condition can ameliorate the impacts of signal obstruction, with the improvements of 30.8%, 8.3% and 5.0% for E, N and U directions based on the integration solution.

INDEX TERMS Velocity determination, multi-GNSS observations, Helmert variance components estimation, velocity vector constraint, Doppler observation, integrated Doppler, carrier phase.

I. INTRODUCTION

BeiDou Navigation Satellite System (BDS) and other Global Navigation Satellite System (GNSS) are promoting innovative development and high-performance positioning, navigation and timing (PNT) services in all-round ways [1]. Therefore, to fully assess and improve the performances of multi-GNSS and multi-frequency observations are the prerequisite for the GNSS applications. It is reported that the GNSS constellations are continuously updated. For example, compared with BDS-2 and other GNSS, the new-generation BDS-3 satellite is equipped with high-stability onboard

clock, inter-satellite link and updates the modulation of transmitting signals [2]. Meanwhile, it is indicated that user range errors (URE) of BDS-3 signals are better than 0.5m, and the superior positioning performance can be obtained, which is mainly benefited from the abundant observations provided by BDS-3 [3], [4], [5]. The civilian signals of BDS-3 satellites reaching up to five frequencies, namely B1C, B1I, B2a, B2b and B3I, are synchronous service. Additionally, the Doppler observations are also contained in multi-GNSS and multi-frequency observations. There are two main methods to use Doppler measurements, called raw Doppler and carrier-phase-derived Doppler [6], [7]. The raw Doppler method is the most widely used cm level technique in GNSS community [8]. Moreover, the

The associate editor coordinating the review of this manuscript and approving it for publication was Venkata Ratnam Devanaboyina .

carrier-phase-derived Doppler method is further obtained to improve the accuracy of velocity determination to mm level [9]. Therefore, to acquire a better performance of location-based service, it is necessary to fully use the merits of carrier phase and Doppler measurements. Moreover, due to the multi-frequency observations modulating by GNSS satellites, it is necessary to further research the carrier phase and Doppler methods [8].

The velocity information is one of essential parameters to describe the states of a kinematics vehicle, which is almost ignored in the area of high-accuracy GNSS researches. Meanwhile, the train positioning, airborne gravimetry, automatic driving and aircraft docking also need high-accuracy velocity information. Traditionally, there are three methods to determine velocity, namely position derivation (PD), Doppler observations (DO) and time-difference carrier phase (TDCP), respectively [10], [11]. According to the related results, it is well known that the precision of TDCP method is optimal, while the DO method can provide a more reliable velocity during the sudden changes of vehicle status [12], [13]. To improve the performance of GNSS velocity determination, impacts of environments on signal attenuation and loss were also analyzed [14]. Then, the combination of robust estimation and Helmert variance components estimation (VCE) algorithm for DO method was discussed [15]. Furthermore, the combination of Doppler and phase observations were studied, which mainly focuses on the choice of the best central difference points [10], [16]. Moreover, the instantaneous velocity estimation can be precisely obtained by the kernel algorithm based on a stand-alone receiver [11]. Meanwhile, the real-time cycle-slip detection and repair approach is proposed with the aid of Doppler observation [17]. As a result, the GNSS observations can be used to accurately determine the vehicle velocity, in which different types observations present different performances.

The ability of velocity determination is one core indicator for the multi-GNSS location-based services. The velocity determinations of BDS-3 multi-frequency observations are fully analyzed based on several static stations, in which a mm/s-level results can be obtained [18]. To improve the reliability of BDS-3 services, the velocity series is also used to detect the abnormal values of BDS-3 satellites [14], [19]. It should be noted that the TDCP method is widely used in velocity determination [19], [20], [21], which is also introduced into some open-source software, such as RTKLIB [22], PPPLib [23], goGPS [24], and iTAG_VAD for velocity determination [25]. However, to further improve the reliability TDCP method, two important issues should be considered: on the one hand, TDCP is more sensitive to the signal obstruction, especially for the condition of less than five satellites. On another hand, Doppler method can provide the instantaneous variation of the carrier phase [25]. However, because of the significant noise, it is difficult to precisely determine velocity with the aid of Doppler method for a high-dynamic instantaneous epoch [7], [15]. Therefore,

the integration of Doppler and phase observations to improve the performance of multi-GNSS velocity determination is proposed in this study.

The main task of this study is to optimize the GNSS velocity determination method based on a single receiver. Apart from Introduction, the improved velocity determination method is presented in Section II, where three parts of equations and the integration solution based on velocity vectors are presented. Then, the experiments and its results analysis based on real data are shown in Section III. Finally, the discussion and conclusions are summarized in Sections IV.

II. IMPROVED VELOCITY DETERMINATION METHOD

To fully use different information of multi-frequency and multi-GNSS signals, the phase and Doppler observations are fused in the determination of velocity parameters based on the vector model. Firstly, the GNSS observation equations can be expressed as follows:

$$\begin{aligned} \rho_r^s &= \lambda_f \cdot \varphi_{r,f}^s + \lambda_f \cdot Amb_{r,f}^s + c \cdot dt^s - c \cdot dt_r \\ &\quad - dtrop_r^s + dion_{r,f}^s + \varepsilon_{r,f}^s \end{aligned} \quad (1)$$

where ρ is the distance between the s -th satellite and the r -th receiver; λ is the wavelength of f -th frequency; φ denotes the phase observations; c , dt^s and dt_r are the speed of light, the clock offsets of satellite and receiver, respectively; Amb , $dtrop$ and $dion$ represent the parameters of ambiguity, troposphere and ionosphere; ε is the model error. Moreover, the derivative of equation (1) can be read as follows:

$$\begin{aligned} e_r^s \cdot V_r^s &= \lambda_f \cdot \dot{\varphi}_{r,f}^s + c \cdot \dot{dt}^s - c \cdot \dot{dt}_r - dtrop_r^s \\ &\quad + dion_{r,f}^s + \dot{\varepsilon}_{r,f}^s \end{aligned} \quad (2)$$

where e_r^s is the direction vector of satellite to receiver; V_r^s denotes the velocity of r -th receiver to s -th satellite, which can be written as $V_r^s = V^s - V_r = [(\dot{X}^s - \dot{X}_r)^2 + (\dot{Y}^s - \dot{Y}_r)^2 + (\dot{Z}^s - \dot{Z}_r)^2]^{1/2}$.

For the high-rate observations, equation (2) can be simplified as follows:

$$e_r^s \cdot V_r^s = \lambda_f \cdot \dot{\varphi}_{r,f}^s + c \cdot \dot{dt}^s - c \cdot \dot{dt}_r + u_{r,f}^s \quad (3)$$

similarly, $u_{r,f}^s$ is the model error, and $\dot{\varphi}_{r,f}^s$ denotes Doppler observations. Meanwhile, to improve the performance of velocity determination model, equation (3) can be decomposed into three-dimension vectors as X, Y and Z directions, which is represented by l , m and ω , respectively.

$$\begin{aligned} &\begin{bmatrix} -e_r^s/l_r^s & 1 & 1 & 1 \\ 1 & -e_r^s/m_r^s & 1 & 1 \\ 1 & 1 & -e_r^s/\omega_r^s & 1 \end{bmatrix} \begin{bmatrix} \dot{X}_r \\ \dot{Y}_r \\ \dot{Z}_r \\ c \cdot \dot{dt}_r \end{bmatrix} \\ &= \begin{bmatrix} \lambda_f \cdot \dot{\varphi}_{r,f}^s + c \cdot \dot{dt}^s + \dot{\varepsilon}_{r,f}^s - e_r^s \cdot \dot{X}^s/l_r^s \\ \lambda_f \cdot \dot{\varphi}_{r,f}^s + c \cdot \dot{dt}^s + \dot{\varepsilon}_{r,f}^s - e_r^s \cdot \dot{Y}^s/m_r^s \\ \lambda_f \cdot \dot{\varphi}_{r,f}^s + c \cdot \dot{dt}^s + \dot{\varepsilon}_{r,f}^s - e_r^s \cdot \dot{Z}^s/\omega_r^s \end{bmatrix} \end{aligned} \quad (4)$$

where $l_r^s = \frac{\dot{X}^s - \dot{X}_{r0}}{V^s - V_{r0}}$, $m_r^s = \frac{\dot{Y}^s - \dot{Y}_{r0}}{V^s - V_{r0}}$, $\omega_r^s = \frac{\dot{Z}^s - \dot{Z}_{r0}}{V^s - V_{r0}}$; moreover, the satellite velocity vector $V^s = [\dot{X}^s \ \dot{Y}^s \ \dot{Z}^s]$ can be obtained from the predicted precise orbit or the broadcast ephemeris, while the velocity of receiver can be set as an approximate value $V_{r0} = [\dot{X}_{r0} \ \dot{Y}_{r0} \ \dot{Z}_{r0}]$. Finally, the velocity of receiver can be estimated based on equations (1)~(4), in which the Doppler observations are used. However, it is indicated that the phase observations can be also used to determine velocity parameters. Therefore, the TDCP solution of the equation (1) is conducted to eliminate the common parameters, such as ambiguity and other error. Therefore, the revised equation at t_k -th epoch can be read as follows:

$$\Delta\rho_r^s(t_{k+1}) = \lambda_f \cdot \Delta\varphi_{r,f}^s(t_{k+1}) - c \cdot \Delta dt_r(t_{k+1}) + \Delta\varepsilon_{r,f}^s(t_{k+1}) \quad (5)$$

It should be noted that the coefficients of the design matrix of three directions for two adjacent epochs can be expressed as the equation (6) with the consideration of the orbit height of navigation satellites [13].

$$\begin{cases} L_r^s(t_k) \approx L_r^s(t_{k+1}) = \frac{X^s(t_{k+1}) - X_{r0}(t_{k+1})}{|X^s(t_{k+1}) - X_{r0}(t_{k+1})|} \\ M_r^s(t_k) \approx M_r^s(t_{k+1}) = \frac{Y^s(t_{k+1}) - Y_{r0}(t_{k+1})}{|X^s(t_{k+1}) - X_{r0}(t_{k+1})|} \\ G_r^s(t_k) \approx G_r^s(t_{k+1}) = \frac{Z^s(t_{k+1}) - Z_{r0}(t_{k+1})}{|X^s(t_{k+1}) - X_{r0}(t_{k+1})|} \end{cases} \quad (6)$$

where the positions of satellite $X^s = [X^s \ Y^s \ Z^s]$ is the known values, while $X_{r0} = [X_{r0} \ Y_{r0} \ Z_{r0}]$ is the approximate positions of receiver. Thus, the equation (5) can be rewritten as follows:

$$\begin{cases} L_r^s(t_k) \cdot (\lambda_f \cdot \Delta\varphi_r^s - c \cdot \Delta dt_r + \Delta\varepsilon_r^s) \\ \quad = \Delta\rho_X(t_k) - \Delta\rho_X(t_{k-1}) \\ M_r^s(t_k) \cdot (\lambda_f \cdot \Delta\varphi_r^s - c \cdot \Delta dt_r + \Delta\varepsilon_r^s) \\ \quad = \Delta\rho_Y(t_k) - \Delta\rho_Y(t_{k-1}) \\ G_r^s(t_k) \cdot (\lambda_f \cdot \Delta\varphi_r^s - c \cdot \Delta dt_r + \Delta\varepsilon_r^s) \\ \quad = \Delta\rho_Z(t_k) - \Delta\rho_Z(t_{k-1}) \end{cases} \quad (7)$$

In equation (7), the increments of displacements are as follows:

$$\begin{aligned} \Delta\rho_X &= [(X^s - X_r)^2]^{1/2}, \Delta\rho_Y = [(Y^s - Y_r)^2]^{1/2}, \\ \Delta\rho_Z &= [(Z^s - Z_r)^2]^{1/2} \end{aligned} \quad (8)$$

For the high-rate observations, $\Delta\rho$ can be represented by the first order Taylor expansion as follows:

$$\begin{cases} \Delta\rho_X(t_k) = \Delta\rho_{X_{r0}}(t_{k-1}) + \frac{\partial\Delta\rho_X(t_{k-1})}{\partial X} \cdot \Delta X_r \\ \Delta\rho_Y(t_k) = \Delta\rho_{Y_{r0}}(t_{k-1}) + \frac{\partial\Delta\rho_Y(t_{k-1})}{\partial Y} \cdot \Delta Y_r \\ \Delta\rho_Z(t_k) = \Delta\rho_{Z_{r0}}(t_{k-1}) + \frac{\partial\Delta\rho_Z(t_{k-1})}{\partial Z} \cdot \Delta Z_r \end{cases} \quad (9)$$

Set the coefficients matrix as follows:

$$\begin{aligned} A_X(t_k) &= \frac{\partial\Delta\rho_X(t_{k-1})}{\partial X}, \quad A_Y(t_k) = \frac{\partial\Delta\rho_Y(t_{k-1})}{\partial Y}, \\ A_Z(t_k) &= \frac{\partial\Delta\rho_Z(t_{k-1})}{\partial Z} \end{aligned} \quad (10)$$

Furthermore, to obtain the velocity parameters, the epoch interval τ should be introduced into equation (7), where the velocity determination equation is read as follows:

$$\begin{aligned} \begin{bmatrix} \frac{A_X(t_k)}{L_r^s(t_k)} & 0 & 0 & -1 \\ 0 & \frac{A_Y(t_k)}{M_r^s(t_k)} & 0 & -1 \\ 0 & 0 & \frac{A_Z(t_k)}{G_r^s(t_k)} & -1 \end{bmatrix} \begin{bmatrix} \dot{X}_r \\ \dot{Y}_r \\ \dot{Z}_r \\ c \cdot \Delta dt_r \end{bmatrix} \\ = \begin{bmatrix} \lambda_f \cdot \dot{\varphi}_{r,f}^s - \frac{1}{L_r^s(t_k)} (X_{r0}(t_{k-1}) - X_r(t_{k-1})) / \tau \\ \lambda_f \cdot \dot{\varphi}_{r,f}^s - \frac{1}{M_r^s(t_k)} (Y_{r0}(t_{k-1}) - Y_r(t_{k-1})) / \tau \\ \lambda_f \cdot \dot{\varphi}_{r,f}^s - \frac{1}{G_r^s(t_k)} (Z_{r0}(t_{k-1}) - Z_r(t_{k-1})) / \tau \end{bmatrix} \end{aligned} \quad (11)$$

Similarly, according to equations (5)~(11), the receiver velocity can be estimated based on the phase observations [23], which can also be obtained with the aid of single epoch difference solution. To fully use Doppler and phase observations, an integrated processing solution is proposed. According to the combination of equations (4) and (11), the normal equations can be constructed as follows:

$$\begin{cases} N_i \hat{x} = B_i \\ N_i = A_i^T P_i A_i \\ B_i = A_i^T P_i L_i \end{cases} \quad (12)$$

where N_i is the coefficients of normal equation; A_i and P_i denote the coefficient matrix of observation equations and its weight, respectively; L_i represents observation minus calculation; \hat{x} is the parameters of velocity and clock offset frequency. Then, based on the combination of two kinds of normal equations, we can obtain the integrated Doppler and phase observations as follows:

$$\begin{cases} N = \sum_{i=1}^2 N_i \\ N \hat{x} = B \\ B = \sum_{i=1}^2 B_i \end{cases} \quad (13)$$

According to the solution of equation (13), the results of velocity and the corrections of observations can be output as:

$$\begin{cases} \hat{x} = N^{-1} B \\ v_i = A_i \hat{x} - L_i \end{cases} \quad (14)$$

To fully fuse the Doppler and phase observations, the Helmert variance components estimation (VCE) is used to accurately calculate the variance factors of unit weight based on two kinds of velocity determination models.

$$\begin{cases} U_1 U_1 \hat{\sigma}_1^2 + U_1 U_2 \hat{\sigma}_2^2 + \dots + U_1 U_k \hat{\sigma}_k^2 = \delta_1^T P_1 \delta_1 \\ U_2 U_1 \hat{\sigma}_1^2 + U_2 U_2 \hat{\sigma}_2^2 + \dots + U_2 U_k \hat{\sigma}_k^2 = \delta_2^T P_2 \delta_2 \\ \dots \\ U_k U_1 \hat{\sigma}_1^2 + U_k U_2 \hat{\sigma}_2^2 + \dots + U_k U_k \hat{\sigma}_k^2 = \delta_k^T P_k \delta_k \end{cases} \quad (15)$$

where $\hat{\sigma}_i^2$ is the estimated variance for i -th observation; δ is the corrected values of observations; U can be expressed as:

$$\begin{cases} U_i U_i = n_i - 2tr(N^{-1}N_i) + tr(N^{-1}N_i)^2 \\ U_i U_j = tr(N^{-1}N_i N^{-1}N_j) \quad i \neq j \end{cases} \quad (16)$$

where n_i is the total number of Doppler and phase equations. Based on the estimated $\hat{\sigma}_i^2$, the improved weight can be updated as follows:

$$P'_i = \frac{P_i}{\hat{\sigma}_i^2} \quad (17)$$

Meanwhile, it should be noted that the velocity parameter is decomposed into three-dimension vectors model in equations (4) and (11). To improve the accuracy of velocity parameters, the vector model can be used to construct the constraint conditions. The velocity vectors are firstly transformed into North-East-Up (N, E, U) directions as follows:

$$\begin{bmatrix} V_N \\ V_E \\ V_U \end{bmatrix} = \begin{bmatrix} -\sin\alpha \cos\beta & -\sin\alpha \sin\beta & \cos\alpha \\ -\sin\beta & \cos\beta & 0 \\ \cos\alpha \cos\beta & \cos\alpha \sin\beta & \sin\alpha \end{bmatrix} \begin{bmatrix} \Delta X_r/\tau \\ \Delta Y_r/\tau \\ \Delta Z_r/\tau \end{bmatrix} \quad (18)$$

where α and β are the geodetic latitude and longitude of receiver. Then, it is not difficult to obtain the geometric relationship between its velocity components and motion direction (heading angle) for a kinematics receiver, where the velocity direction can be represented by the tangent direction of the trajectory. In fact, the additional constraints can be constructed, such as heading angle and pitch angle, to enhance the integration model of Doppler and phase. Meanwhile, to further improve the performances of GNSS velocity determination, additional virtual observations can be added to constraint the unknown parameters. Based on equation (5), we can also obtain the simplified equation as:

$$\lambda_r \cdot \Delta\varphi_r^s - F + Q = -e(t_1) \cdot \Delta X - c \cdot \Delta dt_r \quad (19)$$

where, $F = e(t_2) \cdot X^s(t_2) - e(t_1) \cdot X^s(t_1)$ and $Q = e(t_2) \cdot X_r(t_2) - e(t_1) \cdot X_r(t_1)$; and

$$e(t_i) = \frac{X^s(t_i) - X_r(t_i)}{|X^s(t_i) - X_r(t_i)|} \quad (20)$$

As above mentioned, the improved velocity determination method is constructed by the integration of three parts, namely Doppler, TDCP and constraint condition. To clearly describe the proposed method, the flowchart of improved velocity determination is presented in FIGURE 1.

III. EXPERIMENTS AND RESULTS

According to the proposed method, the integrated GNSS Doppler and phase observations are used to determine the kinematics velocity. To verify and test the proposed method, four experimental schemes of velocity determination are designed in this section.

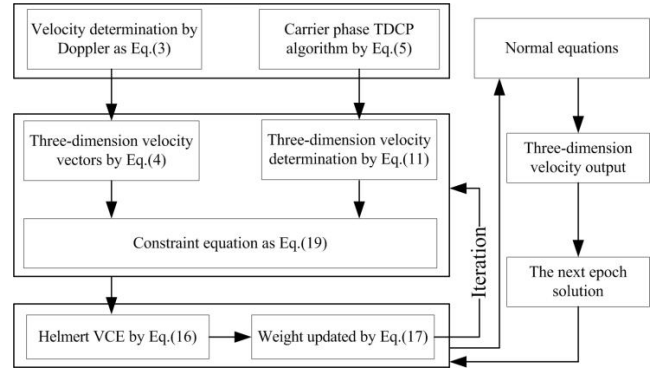


FIGURE 1. The flowchart of the proposed velocity determination solution.

A. RESULTS OF THE WIDELY USED VELOCITY DETERMINATION METHODS

To show the performances of different widely used velocity determination methods, PD, DO and TDCP are used to estimate the velocity parameters, where the double-difference solutions based on Inertial Explorer software package (IE) are set as references of kinematics velocity values. In this case, two GNSS receivers are simultaneous working, one of which is fixed on a moving car and another is set as the reference station on a wide-open roof. The receivers can synchronously decode multi-GNSS and multi-frequency observations, where the time period of observation collection is 8:00-10:00, 16th, July, 2022. In experiments, the cutoff angle and sample rate are set as 5° and 1Hz, respectively. Details about the car trajectory during observations collection are shown in FIGURE 2.



FIGURE 2. The configurations of observation collection and its kinematics trajectory.

According to the collected multi-GNSS observations, three statuses of car trajectory are analyzed, namely linear motion, change direction and signal obstruction. To fully present the results of velocity residuals of PD, DO and TDCP methods, the residuals of different statuses for E, N and U directions are shown in FIGURE 3, FIGURE 4 and FIGURE 5, respectively. Furthermore, the velocity residuals root-mean-square (RMS) of different methods are listed in TABLE 1.

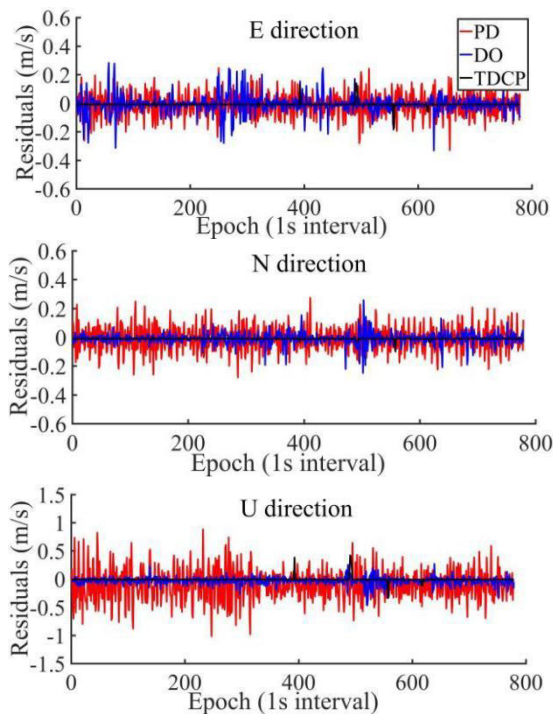


FIGURE 3. The velocity residuals series of PD, DO and TDCP during the linear motion based on multi-GNSS observations.

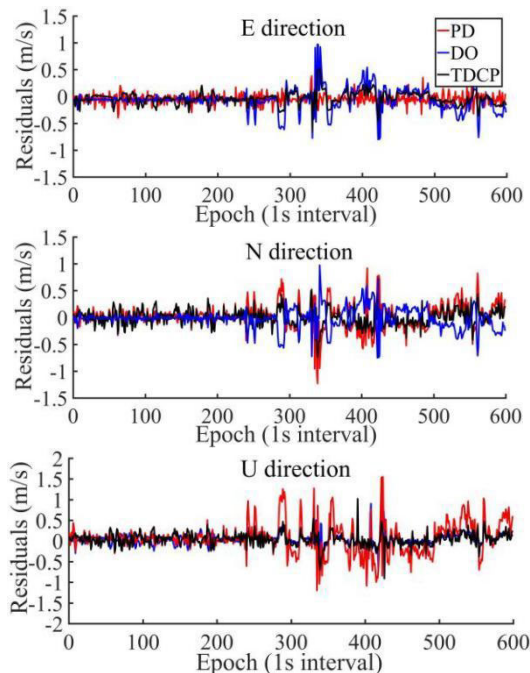


FIGURE 4. The velocity residuals series of PD, DO and TDCP during the change direction based on multi-GNSS observations.

According to the experimental results, the cm/s-level accuracy of velocity determination for different directions can be obtained based on different methods during linear motion. Meanwhile, the TDCP is significantly outperformed in determining velocity, which could be also confirmed based

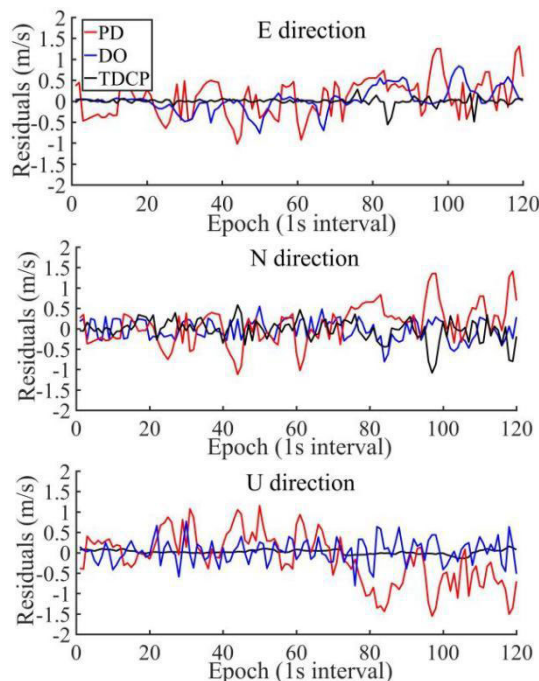


FIGURE 5. The velocity residuals series of PD, DO and TDCP during the signal obstruction based on multi-GNSS observations.

TABLE 1. RMS of velocity residuals for different statuses and methods. Unit: m/s.

Statuses	PD			DO			TDCP		
	E	N	U	E	N	U	E	N	U
Linear motion	0.061	0.070	0.166	0.052	0.039	0.064	0.010	0.004	0.030
Change direction	0.288	0.092	0.274	0.255	0.151	0.082	0.104	0.99	0.028
Signal obstruction	0.168	0.220	0.345	0.801	0.643	0.166	0.228	0.244	0.060

on the status of change direction. However, it is indicated that the signal obstruction imposes a direct impact on the accuracy of velocity determination. Because of the characteristic of different methods, different results of velocity can be obtained. In general, two types of observations are used, namely Doppler and phase, where the noise of Doppler observations is more obvious than that of phase observations. Nevertheless, a similar level of velocity accuracy is shown in TABLE 1, which suggested that the Doppler observations are more stabler in some suddenly changed statuses. To improve the performance of GNSS velocity determinations with the single receiver, it is necessary to integrate the Doppler and phase observations, which performances are shown in next section. It should be noted that the results of the proposed method are not included in experiments: firstly, this section is to test the performances of traditional velocity determination methods, where the proposed method will be further discussed in next section; secondly, because of the complex road condition of observation collection, the continuous epochs are always interrupted, which imposes a

significant impact on the accuracy of heading angle; thirdly, to distinguish the results of PD, DO and TDCP, the proposed method is analyzed in next section, and the results are similar with the TDCP and a slight improvement can be acquired as the restriction of heading angle.

B. RESULTS OF THE PROPOSED VELOCITY DETERMINATION METHODS

The integrated processing of Doppler and phase observations is conducted to verify the proposed velocity determination methods. Strategies of observations collection are the same as the first experiments, while the kinematics trajectory is changed to the road around the Institute of Surveying and Mapping Geographic Information. The car trajectory is shown in FIGURE 6, including different statuses of moving.



FIGURE 6. The trajectory of car moving around the institute of surveying and mapping geographic information.

Similarly, the velocity solutions of IE software are provided for reference. The purpose of this study is to improve the velocity determination performance of GNSS single receiver, and fully use the different types of observations. Therefore, the schemes of Helmert VCE (Helmert) and 1:1 combination (1:1) solutions are analyzed, where 1:1 represents the equivalent weight model for Doppler and phase observations. Moreover, the PD, DO and TDCP methods based on GNSS observations are also listed in this experiment. In FIGURE 7, the velocity residuals series of five methods are presented, which is conducted under the normal condition (N). To further test the proposed integrated method, the signal obstruction condition (AN) is also simulated and its residuals series of velocity are shown in FIGURE 8.

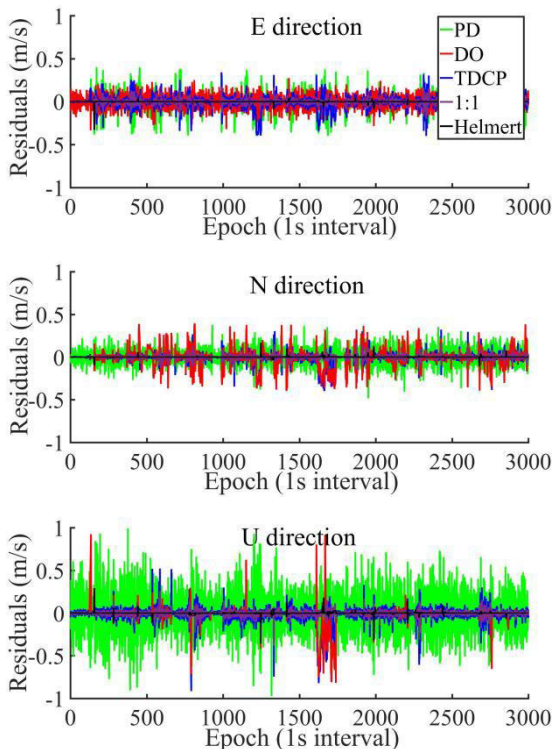


FIGURE 7. Velocity residuals of PD, DO, TDCP, integration (1:1) and Helmert VCE (Helmert) solutions.

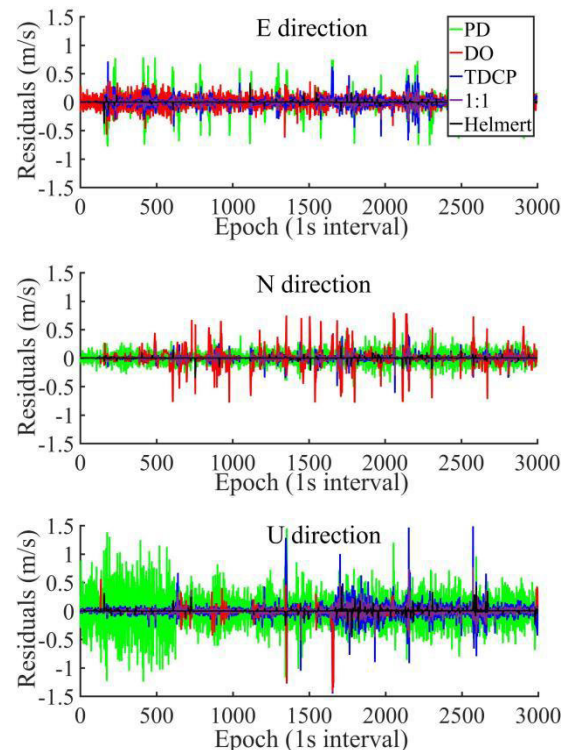


FIGURE 8. Velocity residuals of PD, DO, TDCP, integration (1:1) and Helmert VCE (Helmert) solutions under signal obstruction condition.

To explain the condition of the signal obstruction, the PDOP values of normal and signal obstruction solutions is calculated in FIGURE 9. Moreover, the weight coefficients of Helmert VCE for Doppler and phase observations are also listed in FIGURE 9. Certainly, the Helmert VCE method performs a smaller velocity residual than phase-only, Doppler-only and 1:1 integration. For the sake of describing the impacts of different types of observations on integration methods, it is found that the values of weight coefficients for phase observation are typically higher than that of Doppler, which is near to zero for the signal obstruction mode. Because of the higher accuracy of phase observations, the weight of phase is bigger in the integration method for most of epochs.

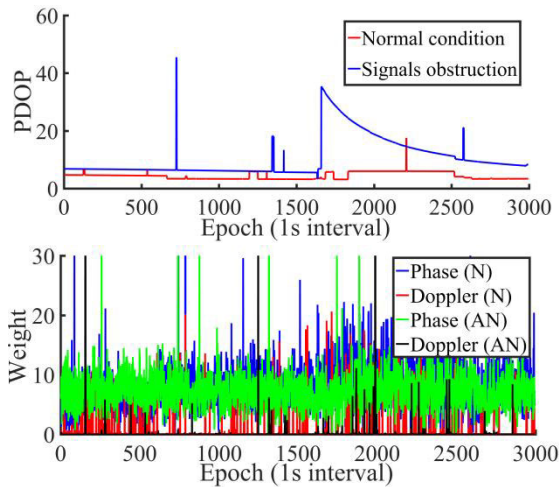


FIGURE 9. PDOP values and weight coefficients of phase and Doppler observations for normal (N) and signal obstruction (AN) conditions.

It is indirectly demonstrated that the simple combination of Doppler and phase observations, such as 1:1 strategy, cannot obtain the optimal velocity results. Additionally, the RMS of velocity residuals based on different solutions and its improvements are listed in TABLE 2, where the normal and signal obstruction conditions are analyzed respectively. According to the experimental results, the combination of Doppler and phase observations indeed outperforms in aspect of PD-only, Doppler-only and TDCP-only. For the Helmert VCE method in normal condition, improvements with 94.1%, 93.9% and 89.5% can be obtained for E, N and U directions, compared with Doppler-only method, where the low-accuracy PD-only method is also listed. Although the velocity accuracy of signal obstruction condition reduced, a cm/s-level accuracy can still be obtained based on the integration of Doppler and phase observations. Meanwhile, the improvements are reached up to 89.7%, 90.1% and 69.4% for E, N and U directions by using the Helmert integration under the condition of signal obstruction. Thereby, the integrated processing of GNSS Doppler and phase should be used in determining velocity, in which the Helmert VCE can adaptively adjust the weight of two types of observations, and a better result is obtained.

To further improve the stability of GNSS velocity determination, a constraint condition is designed by taking the original phase observations into consideration as expressed in equation (19). Therefore, to test the reliability of introducing constraint on determining velocity, the same observations collected around the Institute of Surveying and Mapping Geographic Information are used. In experiments, the constraint is added into the solution of Helmert VCE, where the normal condition and signal obstruction are set as two scenarios. The velocity residuals based on Helmert VCE method are shown in FIGURE 10. Moreover, the RMS values of constraint and non-constraint velocity determinations are shown in TABLE 3.

TABLE 2. RMS of velocity residuals based on different solutions and its improvements. Unit: m/s.

Normal condition (N)						
Directions	E	Imp.	N	Imp.	U	Imp.
Doppler-only	0.101	/	0.082	/	0.095	/
TDCP-only	0.056	/	0.062	/	0.098	/
PD-only	0.126	/	0.114	/	0.132	/
1:1 integration	0.019	81.2%	0.021	74.4%	0.029	69.5%
Helmert integration	0.006	94.1%	0.005	93.9%	0.010	89.5%
Signal obstruction condition (AN)						
Directions	E	Imp.	N	Imp.	U	Imp.
Doppler-only	0.145	/	0.101	/	0.072	/
TDCP-only	0.072	/	0.055	/	0.122	/
PD-only	0.268	/	0.206	/	0.044	/
1:1 integration	0.032	77.9%	0.023	77.2%	0.056	22.2%
Helmert integration	0.015	89.7%	0.010	90.1%	0.022	69.4%

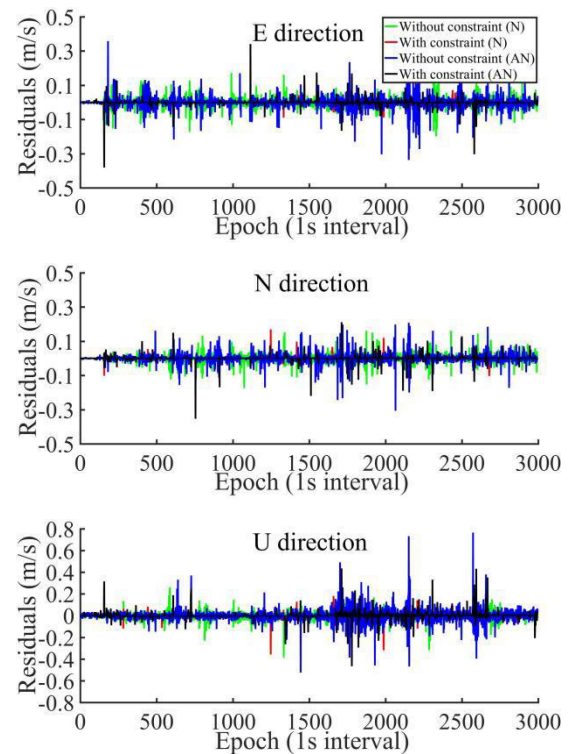


FIGURE 10. The velocity residuals of Helmert VCE solutions with and without the constraint under normal (N) and abnormal (AN) conditions.

TABLE 3. RMS of velocity residuals based on constraint and its improvements. Unit: m/s.

Solutions	Without constraint			With constraint					
	E	N	U	E	Imp.	N	Imp.	U	Imp.
Signal obstruction	0.013	0.012	0.020	0.009	30.8%	0.011	8.3%	0.019	5.0%
Normal condition	0.006	0.005	0.011	0.004	33.3%	0.004	20.0%	0.009	18.2%

According to the results presented in TABLE 3 and FIGURE 10, it is indicated that the accuracy of velocity determination for E and N directions is slightly changes,

where the improvements 30.8% and 33.3% in V_E are presented based on the signal obstruction and normal condition. Meanwhile, the improvements of 8.3% and 5.0% for N and U directions can be obtained under the condition of signal obstruction. The constraint condition is constructed based on the original phase observations, which can be precisely obtained. Therefore, the velocity accuracy is impacted by the reliability of constraint condition, which can directly improve the velocity performances under the signal obstruction.

As one of main featured abilities of multi-GNSS system, the multi-frequency signals can be transmitted, such as B1I, B3I, B1C, B2a and B2b for BDS-3, L1 C/A, L1C, L2C, and L5 signals for GPS, and E1, E5a, E5b, E5, and E6 for Galileo. In the velocity determination experiments, the observations of multi-frequency phase and Doppler are used to test the proposed velocity determination method. To show the performances of multi-frequency data, the phase residuals of different frequencies for BDS-3, GPS and Galileo observations are shown in FIGURE 11, FIGURE 12 and FIGURE 13, respectively.

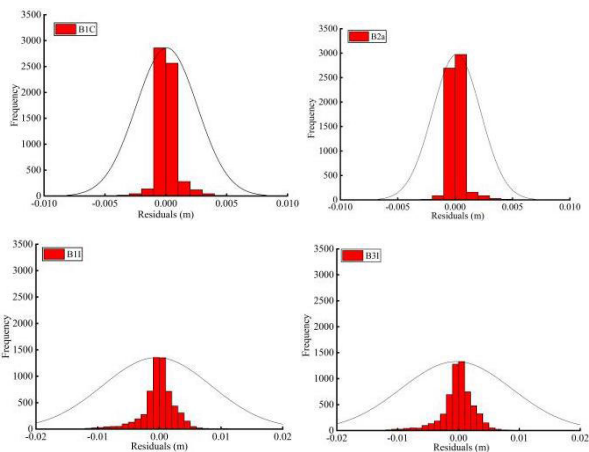


FIGURE 11. The BDS-3 phase residuals distribution of velocity determination.

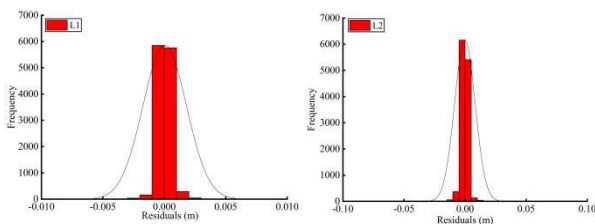


FIGURE 12. The GPS phase residuals distribution of velocity determination.

Moreover, the velocity residuals RMS of different GNSS by integrating with Doppler observations are listed in TABLE 4, where a cm/s-level accuracy of velocity determination can be obtained for all systems.

According to the testes of multi-GNSS and multi-frequency observations based on the proposed integrated Doppler and phase method, it is indicated that velocity

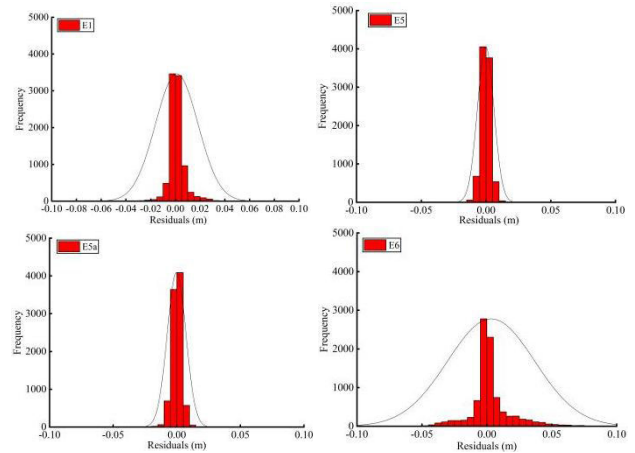


FIGURE 13. The Galileo phase residuals distribution of velocity determination.

TABLE 4. The velocity residuals RMS based on different GNSS systems. Unit: m/s.

Systems	E	N	U
BDS-3	0.012	0.016	0.058
GPS	0.013	0.011	0.069
Galileo	0.033	0.018	0.072
Glonass	0.039	0.026	0.092

residuals present the Normal distributions for all phase observations, where the velocity residuals RMS of each system are similar with. Moreover, from TABLE 4, it is found that the BDS-3 slightly outperforms GPS, Galileo and Glonass, which is mainly benefited from the lower noise for the new-generation BDS-3 satellites [5], [26]. Furthermore, there are not significant differences between BDS-3, GPS and Galileo in determining velocity, while the Glonass should be carefully processed. All experiments are conducted based on self-developed tool, which is a multi-frequency and multi-GNSS velocity and acceleration determination software. In addition, the computational complexity of the proposed method is also analyzed based on the velocity determination software. In TABLE 5, the averaged time-consuming of single-epoch solution for different methods is presented by marking the time log file. It is indicated that the time-consuming of the proposed method is slightly higher than that of traditional method. However, compared with the time interval of observation collection, the time-consuming for different methods can be ignored.

C. DISSCUSSION

Considering the complexity of the navigation environment, a constraint condition is constructed using the original phase observations to increase the performance of velocity determination. The authors proposed that combining GNSS carrier phase and Doppler observations can improve the accuracy of the velocity determination [3]. We use the improved Helmert VCE method with the horizontal plane

TABLE 5. The averaged time-consuming of single-epoch solution for different method (s).

Statuses	PD	DO	TDCP	New method
Linear motion	0.004	0.001	0.008	0.011
Change direction	0.006	0.001	0.009	0.013
Signal obstruction	0.005	0.004	0.009	0.012

constraint condition to determine the reasonable weights and enhance the reliability, and redundancy of the model to achieve high-precision speed information to avoid the abnormal information or no data caused by the signal obstruction, which ensures velocity information reliability of navigation and positioning.

The PD, DO and TDCP methods are applied in navigation and positioning, which can only use one of positions, Doppler and carrier phase to estimate velocity. These methods need to integrate Doppler and phase observations, which will improve model redundancy and velocity reliability. Furthermore, when we drive the car with one receiver in the signal obstruction environment, that will seriously affect the velocity results' accuracy. However, the proposed method avoids all the above-mentioned problems and provides a new solution for velocity determination.

IV. CONCLUSION

This paper proposes an improved velocity determination method based on multi-GNSS and multi-frequency observations, in which the Doppler and phase observations are integrated processing. To combine the GNSS phase and Doppler observations precisely, the Helmert VCE method is used in the improved method. Furthermore, a constraint condition is constructed to increase the reliability of velocity determination in the complicated environment, such as the signal obstruction. To test and verify the proposed method, four schemes of experiments are conducted. According to the results of different schemes, the conclusions can be summarized as:

- 1) Different accuracy is shown based on PD, DO and TDCP, and a cm/s-level of velocity accuracy can be obtained under the normal condition, while the accuracy is significantly reduced for some complicated conditions. Therefore, it is essential to integrate different observations.
- 2) The velocity accuracy can be obviously improved based on the integrated processing of GNSS Doppler and phase observations. Moreover, the Helmert VCE scheme is better than the simple combination (1:1 integration). Compared with the Doppler-only solution, improvements with 94.1%, 93.9% and 89.5% can be obtained for E, N and U directions, respectively, under the normal conditions. Meanwhile, improvements with

89.7%, 90.1% and 69.4% for E, N and U directions can be output under the signal obstruction conditions.

- 3) Additionally, a constraint condition is constructed to improve the integrated model. It is suggested that the velocity of E, N and U directions can be improved with 30.8%, 8.3% and 5.0% under the abnormal condition. Furthermore, the multi-GNSS phase observations are also tested. There are not significantly differences found in velocity residuals distributions.

The purpose of this study is to improve the velocity determination performance of GNSS single station. Compared with traditional PD, DO and TDCP methods, the integrated Doppler and phase observations based on Helmert VCE is designed and analyzed. In the next step, the integration of multi-frequency phase and Doppler observations by PPP solution will be further studied.

REFERENCES

- [1] Y. Yang, L. Liu, J. Li, Y. Yang, T. Zhang, Y. Mao, B. Sun, and X. Ren, "Featured services and performance of BDS-3," *Sci. Bull.*, vol. 66, no. 20, pp. 2135–2143, Oct. 2021.
- [2] Y. Yang, C. Yang, and X. Ren, "PNT intelligent services," *Acta Geodaetica et Cartographica Sinica*, vol. 50, no. 8, pp. 1006–1012, 2021, doi: 10.11947/j.AGCS.2021.20210051.
- [3] C. Hu, Q. Wang, and A. H. Moraleda, "Improved mitigation method for the multipath delays of BDS-3 code observations with the aid of a sparse modeling algorithm," *J. Sensors*, vol. 2021, pp. 1–19, Sep. 2021, doi: 10.1155/2021/9947704.
- [4] X. Li, X. Li, J. Huang, Z. Shen, B. Wang, Y. Yuan, and K. Zhang, "Improving PPP-RTK in urban environment by tightly coupled integration of GNSS and INS," *J. Geodesy*, vol. 95, no. 12, pp. 1–18, Dec. 2021, doi: 10.1007/s00190-021-01578-6.
- [5] Z. Wu, Q. Wang, C. Hu, Z. Yu, and W. Wu, "Modeling and assessment of five-frequency BDS precise point positioning," *Satell. Navigat.*, vol. 3, pp. 1–14, May 2022.
- [6] A. M. Bruton, C. L. Glennie, and K. P. Schwarz, "Differentiation for high-precision GPS velocity and acceleration determination," *GPS Solutions*, vol. 2, no. 4, pp. 7–21, Apr. 1999.
- [7] M. E. Cannon, G. Lachapelle, M. C. Szarmes, J. M. Hebert, J. Keith, and S. Jakerst, "DGPS kinematic carrier phase signal simulation analysis for precise velocity and position determination," *Navigation*, vol. 44, no. 2, pp. 231–245, Jun. 1997.
- [8] Q. Wang, T. Xu, and G. Xu, "Adaptively changing reference station algorithm and its application in GPS long rang airborne kinematics relative positioning," *Acta Geodaetica et Cartographica Sinica*, vol. 40, no. 4, pp. 429–434, 2011.
- [9] P. Freda, A. Angrisano, S. Gaglione, and S. Troisi, "Time-differenced carrier phases technique for precise GNSS velocity estimation," *GPS Solutions*, vol. 19, no. 2, pp. 335–341, Apr. 2015.
- [10] Q. Wang and T. Xu, "A precision acceleration determination method based on combining GPS carrier phase and Doppler," *Proc. Eng.*, vol. 16, pp. 737–744, Jan. 2011, doi: 10.1016/j.proeng.2011.08.1149.
- [11] G. Chang, N. Qian, and C. Chen, "Precise instantaneous velocimetry and accelerometry with a stand-alone GNSS receiver based on sparse kernel learning," *Measurement*, vol. 159, Jul. 2020, Art. no. 107803, doi: 10.1016/j.measurement.2020.107803.
- [12] H. He, Y. Yang, and Z. Sun, "A comparison of several approaches for velocity determination with GPS," *Acta Geodaetica et Cartographica Sinica*, vol. 31, no. 3, pp. 217–221, 2002.
- [13] R. Sun, Q. Cheng, and J. Wang, "Precise vehicle dynamic heading and pitch angle estimation using time-differenced measurements from a single GNSS antenna," *GPS Solutions*, vol. 24, no. 3, pp. 1–9, Jul. 2020, doi: 10.1007/s10291-020-01000-2.
- [14] H. Liu, H. Wei, and X. Zou, "Precise GNSS phase velocity determination for GRACE follow-on satellites," *Acta Geodaetica et Cartographica Sinica*, vol. 50, no. pp. 1772–1779, 2021, doi: 10.11947/j.AGCS.2021.20200140.

- [15] K. He, T. Xu, C. Foste, S. Petrovic, Z. Wang, Y. Tian, and F. Flechtner, "Integrated GNSS Doppler velocity determination for GEOHALO airborne gravimetry," *GPS Solutions*, vol. 25, p. 146, Oct. 2021, doi: [10.1007/s10291-021-01183-2](https://doi.org/10.1007/s10291-021-01183-2).
- [16] Q. Wang and T. Xu, "Combining GPS carrier phase and Doppler observations for precise velocity determination," *Sci. China Phys., Mech. Astron.*, vol. 54, no. 6, pp. 1022–1028, Jun. 2011, doi: [10.1007/s11433-011-4331-z](https://doi.org/10.1007/s11433-011-4331-z).
- [17] Z. Shi, X. Dong, Z. Qian, X. Sun, and Y. Hu, "A new real-time cycle slip detection and repair approach based on BDS dual-frequency carrier phase and Doppler observations," *IET Radar, Sonar Navigation*, vol. 16, pp. 51–63, Jan. 2021.
- [18] T. Geng, Z. Ding, X. Xie, and Y. Lv, "Multi-frequency and Multi-GNSS velocity estimation with time differenced carrier phase method," *Geomatics Inf. Sci. Wuhan Univ.*, vol. 48, no. 2, pp. 206–213, 2021, doi: [10.13203/j.whugis20200226](https://doi.org/10.13203/j.whugis20200226).
- [19] R. Tu, R. Zhang, P. Zhang, J. Han, L. Fan, and X. Lu, "Recover the abnormal positioning, velocity and timing services caused by BDS satellite orbital maneuvers," *Satell. Navigat.*, vol. 2, no. 1, pp. 1–11, Dec. 2021, doi: [10.1186/s43020-021-00048-w](https://doi.org/10.1186/s43020-021-00048-w).
- [20] G. Colosimo, M. Crespi, and A. Mazzoni, "Real-time GPS seismology with a stand-alone receiver: A preliminary feasibility demonstration," *J. Geophys. Res., Solid Earth*, vol. 116, no. 11, Nov. 2011, Art. no. B11302, doi: [10.1029/2010JB007941](https://doi.org/10.1029/2010JB007941).
- [21] Y. Zhao, "Applying time-differenced carrier phase in nondifferential GPS/IMU tightly coupled navigation systems to improve the positioning performance," *IEEE Trans. Veh. Technol.*, vol. 66, no. 2, pp. 992–1003, Feb. 2017, doi: [10.1109/TVT.2016.2558206](https://doi.org/10.1109/TVT.2016.2558206).
- [22] T. Takasu and A. Yasuda, "Development of the low-cost RTK-GPS receiver with an open source program package RTKLIB," in *Proc. Int. Symp. GPS/GNSS*, Seogwiposi Jungmundong, (South) Korea, Nov. 2009, pp. 1–6.
- [23] C. Chen and G. Chang, "PPPLib: An open-source software for precise point positioning using GPS, BeiDou, galileo, GLONASS, and QZSS with multi-frequency observations," *GPS Solutions*, vol. 25, no. 1, pp. 1–7, Nov. 2020, doi: [10.1007/s10291-020-01052-4](https://doi.org/10.1007/s10291-020-01052-4).
- [24] A. M. Herrera, H. F. Suhandri, E. Realini, M. Reguzzoni, and M. C. de Lacy, "goGPS: Open-source MATLAB software," *GPS Solutions*, vol. 20, no. 3, pp. 595–603, 2016, doi: [10.1007/s10291-015-0469-x](https://doi.org/10.1007/s10291-015-0469-x).
- [25] L. Serrano, D. Kim, and R. Langley, "A single GPS receiver as a real-time, accurate velocity and acceleration sensor," in *Proc. GNSS*, Long Beach, CA, USA, Sep. 2004, pp. 2021–2034.
- [26] J. Guo, X. Xu, Q. Zhao, and J. Liu, "Precise orbit determination for quad-constellation satellites at Wuhan university: Strategy, result validation, and comparison," *J. Geodesy*, vol. 90, no. 2, pp. 143–159, Feb. 2016, doi: [10.1007/s00190-015-0862-9](https://doi.org/10.1007/s00190-015-0862-9).



YUNLONG ZHANG received the Ph.D. degree in road and railway engineering from Beijing Jiaotong University, Beijing, China, in 2018. He is currently a Senior Engineer with China Railway Design Corporation and the Deputy Director of the Tianjin Key Laboratory of Rail Transit Navigation Positioning and Spatio-Temporal Big Data Technology. His main research interests include Beidou + Seamless PNT, Beidou survey, and Beidou navigation and positioning.

• • •